© 2016. Published by The Company of Biologists Ltd | Journal of Cell Science (2016) 129, 4034-4045 doi:10.1242/jcs.195032

RESEARCH ARTICLE

Acsl, the *Drosophila* ortholog of intellectual-disability-related ACSL4, inhibits synaptic growth by altered lipids

Yan Huang[1], Sheng Huang[1,2,*], Sin Man Lam[1], Zhihua Liu[1,‡], Guanghou Shui[1] and Yong Q. Zhang[1,§]

ABSTRACT

Nervous system development and function are tightly regulated by metabolic processes, including the metabolism of lipids such as fatty acids. Mutations in long-chain acyl-CoA synthetase 4 (ACSL4) are associated with non-syndromic intellectual disabilities. We previously reported that Acsl, the *Drosophila* ortholog of mammalian ACSL3 and ACSL4, inhibits neuromuscular synapse growth by suppressing bone morphogenetic protein (BMP) signaling. Here, we report that Acsl regulates the composition of fatty acids and membrane lipids, which in turn affects neuromuscular junction (NMJ) synapse development. *Acsl* mutant brains had a decreased abundance of C16:1 fatty acyls; restoration of Acsl expression abrogated NMJ overgrowth and the increase in BMP signaling. A lipidomic analysis revealed that Acsl suppressed the levels of three lipid raft components in the brain, including mannosyl glucosylceramide (MacCer), phosphoethanolamine ceramide and ergosterol. The MacCer level was elevated in *Acsl* mutant NMJs and, along with sterol, promoted NMJ overgrowth, but was not associated with the increase in BMP signaling in the mutants. These findings suggest that Acsl inhibits NMJ growth by stimulating C16:1 fatty acyl production and concomitantly suppressing raft-associated lipid levels.

KEY WORDS: Neuromuscular junction, ACSL, Long-chain acyl-CoA synthetase, Fatty acid, Lipid, Synaptic growth

INTRODUCTION

Lipids are essential membrane components that have crucial roles in neural development and function (Davletov and Montecucco, 2010; Lauwers et al., 2016). Dysregulation of lipid metabolism underlies a wide range of human neurological diseases including neurodegeneration and intellectual disability (Bazinet and Laye, 2014; Najmabadi et al., 2011; Sivachenko et al., 2016). Acyl-CoA synthetase long-chain family member 4 (ACSL4) is the first gene in fatty acid metabolism associated with non-syndromic intellectual disability (Longo et al., 2003; Meloni et al., 2002). ACSL4 protein has two variants: a ubiquitously expressed short form (Kang et al., 1997), and a brain-specific long form that is highly expressed in the hippocampus, a crucial region for memory (Meloni et al., 2002). Indeed, ACSL4 has been shown to play an important role in synaptic spine formation (Meloni et al., 2009). However, it is unclear how mutations in ACSL4 lead to intellectual disability.

There are 26 genes encoding acyl-CoA synthetases (ACSs) in humans. Each of the enzymes has distinct substrate preferences for fatty acid with various lengths of aliphatic carbon chains. In contrast, there are 13 ACS genes in the *Drosophila* genome (Watkins et al., 2007). ACSs convert free fatty acids into acyl-CoAs for lipid synthesis, fatty acid degradation or membrane lipid remodeling (Mashek et al., 2007). For example, ACSL4 converts long-chain fatty acids (LCFAs; aliphatic tails longer than 12 carbons), preferentially arachidonic acid (C20:4), into LCFA-CoAs that are incorporated into glycerol-phospholipids (GPLs) and neutral lipids in non-neuronal cells (Golej et al., 2011; Kuch et al., 2014). The mechanism of how fatty acids and fatty-acid-modifying enzymes affect lipid composition, and thereby modulate development processes, is beginning to be understood in lower model organisms (Kniazeva et al., 2012; Zhang et al., 2011; Zhu et al., 2013).

Synaptic growth is required for normal brain function such as learning and memory. Many neurological disorders including intellectual disability are associated with synaptic defects (Zoghbi and Bear, 2012). The *Drosophila* neuromuscular junction (NMJ) is a powerful system for studying the mechanisms that regulate synaptic growth (Collins and DiAntonio, 2007; Deshpande and Rodal, 2016). *Drosophila* Acsl, also known as dAcsl, is the ortholog of mammalian ACSL3 and ACSL4 (Zhang et al., 2009). We have previously reported that Acsl affects axonal transport of synaptic vesicles and inhibits NMJ growth by inhibiting bone morphogenetic protein (BMP) signaling (Liu et al., 2011, 2014). However, how Acsl affects lipid metabolism and the role of Acsl-regulated lipid metabolism in synapse development are largely unknown.

In the present study, we demonstrate that Acsl positively regulates the abundance of the LCFA palmitoleic acid (C16:1) in the brain. Reduced levels of C16:1 in *Acsl* mutants led to NMJ overgrowth and enhanced BMP signaling. A lipidomic analysis revealed that mannosyl glucosylceramide (MacCer), phosphoethanolamine ceramide (CerPE, the *Drosophila* analog of sphingomyelin) and ergosterol levels were increased in *Acsl* mutant brains. Genetic and pharmacological analyses further showed that the increased level of MacCer and sterol underlie the NMJ overgrowth in *Acsl* mutants in a pathway parallel to BMP signaling. These results indicate that Acsl regulates fatty acid and sphingolipid levels to modulate growth signals and NMJ growth, providing insight into the pathogenesis of ACSL4-related intellectual disability.

RESULTS

Acsl enzymatic activity is required for NMJ development

Three different mutations in ACSL4 have been identified in patients with non-syndromic intellectual disability that are linked to reduced enzymatic activity (Longo et al., 2003; Meloni et al., 2002), suggesting that the enzymatic function of ACSL4 is required for normal brain function. Our previous study showed that

[1]State Key Laboratory for Molecular and Developmental Biology, Institute of Genetics and Developmental Biology, Chinese Academy of Sciences, Beijing 100101, China. [2]Sino-Danish College, Sino-Danish Center for Education and Research, University of Chinese Academy of Sciences, Beijing 100190, China. *Present address: Institute of Biology, Freie Universität Berlin, Berlin 14195, Germany ‡Present address: Department of Neurobiology, Harvard Medical School, Boston, MA 02115, USA

Author for correspondence (yqzhang@genetics.ac.cn)

Y.Q.Z., 0000-0003-0581-4882

Received 15 July 2016; Accepted 16 September 2016

Journal of Cell Science

Journal of Cell Science (2016) 129, 4034-4045 doi:10.1242/jcs.195032

Drosophila Acsl inhibits NMJ synaptic growth (Liu et al., 2014). Weak hypomorphic $Acsl^{8}/Acsl^{05847}$ mutants display synaptic overgrowth with excess satellite boutons, whereas the strong hypomorphic $Acsl^{05847}/Acsl^{KO}$ combination results in more severe NMJ overgrowth phenotype in anterior abdominal segments (Fig. 1A–C,J–L; Liu et al., 2014). We assessed whether the ACSL enzymatic activity is required for normal NMJ growth by treating wild-type larvae with the general ACSL inhibitor triacsin C and the ACSL4-specific inhibitor rosiglitazone (Kim et al., 2001; Van Horn et al., 2005). These larvae showed more total boutons and satellite boutons upon treatment than that in control larvae (Fig. 1G–I,J). Accordingly, neuronal overexpression of wild-type but not disease-causing mutant ACSL4, rescued the NMJ overgrowth in $Acsl^{KO}/Acsl^{05847}$ mutants (Fig. 1D–J). These results demonstrate that Acsl enzymatic activity is required for inhibiting synapse growth at NMJ terminals.

Acsl localizes at ER and peroxisomes in neurons and a subset of non-neuronal cells, respectively

ACSs might provide acyl-CoAs for mitochondrial β-oxidation, peroxisomal oxidation or lipid synthesis in the endoplasmic reticulum (ER), depending on which organelle that a specific ACS associates with (Fig. 2H; Coleman et al., 2000; Ellis et al., 2010; Mashek et al., 2007). Many studies have reported that both rat ACSL4 and *Drosophila* Acsl are enriched in the ER (Lewin et al., 2002; Meloni et al., 2009; O'Sullivan et al., 2012; Zhang et al., 2009), suggesting that they have a role in lipid synthesis. Indeed, both ACSL4 and Acsl positively regulate lipid biosynthesis (Golej et al., 2011; Kuch et al., 2014; Zhang et al., 2009). In addition, ACSL4 is also enriched in peroxisomes of rat liver (Lewin et al., 2002). To clarify the metabolic function of Acsl in the brain, we examined Acsl localization in various organelles of motor neurons in the ventral nerve cord (VNC). The expression of Acsl–Myc driven by motor-neuronal *OK6-Gal4* overlapped completely with proteins tagged with the ER retention signal KDEL, but only partly overlapped with the mitochondrial marker mito-GFP, the peroxisomal marker GFP–SKL and the Golgi marker anti-GM130 (Fig. 2A–D″). The ER location of Acsl suggests that Acsl primarily activates fatty acids for lipid synthesis in the nervous system.

Notably, Acsl–Myc driven by ubiquitous *act-Gal4* was highly expressed in peripheral nerves and a few Elav-negative non-neuronal cells in the VNC (Fig. 1E,G), and weakly expressed in a subset of Elav-positive neurons (Fig. 1E,F). The punctate pattern of

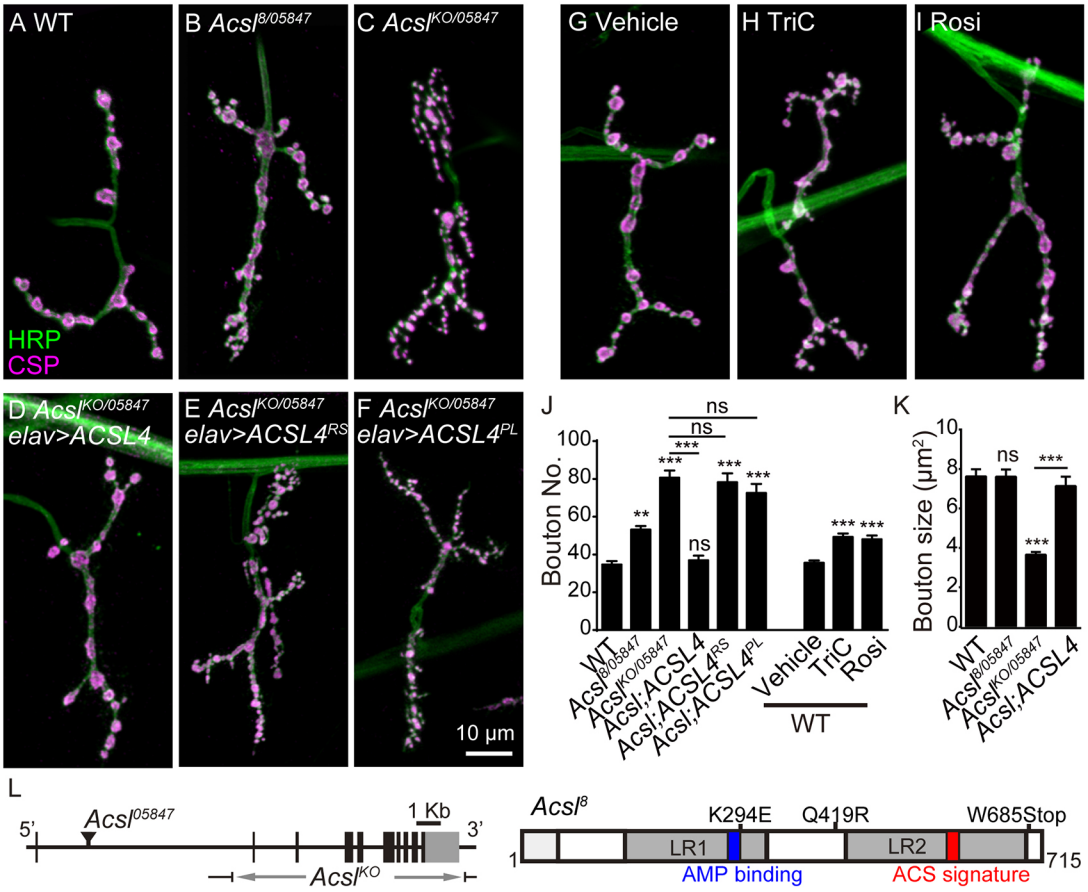

Fig. 1. Enzymatic activity of Acsl is required for NMJ development. (A–F) Images of NMJ4 in segments A2 or A3 stained with anti-HRP and anti-CSP in wild-type (WT, A), $Acsl^{8}/Acsl^{05847}$ (B), $Acsl^{KO}/Acsl^{05847}$ (C), *elav-Gal4*/+; $Acsl^{KO}/Acsl^{05847}$; *UAS-ACSL4*/+ (D) *elav-Gal4*/+; $Acsl^{KO}/Acsl^{05847}$; *UAS-ACSL4*/+ (R570S) (E), and *elav-Gal4*/+; $Acsl^{KO}/Acsl^{05847}$; *UAS-ACSL4*/+ (P375 L) (F) in third-instar larvae. (G–I) Wild-type larvae were treated with vehicle (0.5% DMSO) (G), 100 µM Triacsin C (TriC) (H), and 300 µM rosiglitazone (Rosi) (I). (J,K) Quantifications of the bouton number (J) and bouton size (K) of NMJ4. Results are mean±s.e.m. for $n \geq 12$ larvae. $^{**}P<0.01$; $^{***}P<0.001$; ns, not significant (one-way ANOVA with Tukey post hoc tests). (L) Schematic representation of the genomic structure of *Acsl*. Left, introns are indicated by horizontal lines, exons by vertical lines or boxes, and coding regions by black boxes. The insertion sites of *P* element line 05847 and deleted region of $Acsl^{KO}$ are indicated. Right, the three point mutations of the $Acsl^{8}$ allele are indicated on the protein domains of Acsl. LR, luciferase domain.

Journal of Cell Science (2016) 129, 4034-4045 doi:10.1242/jcs.195032

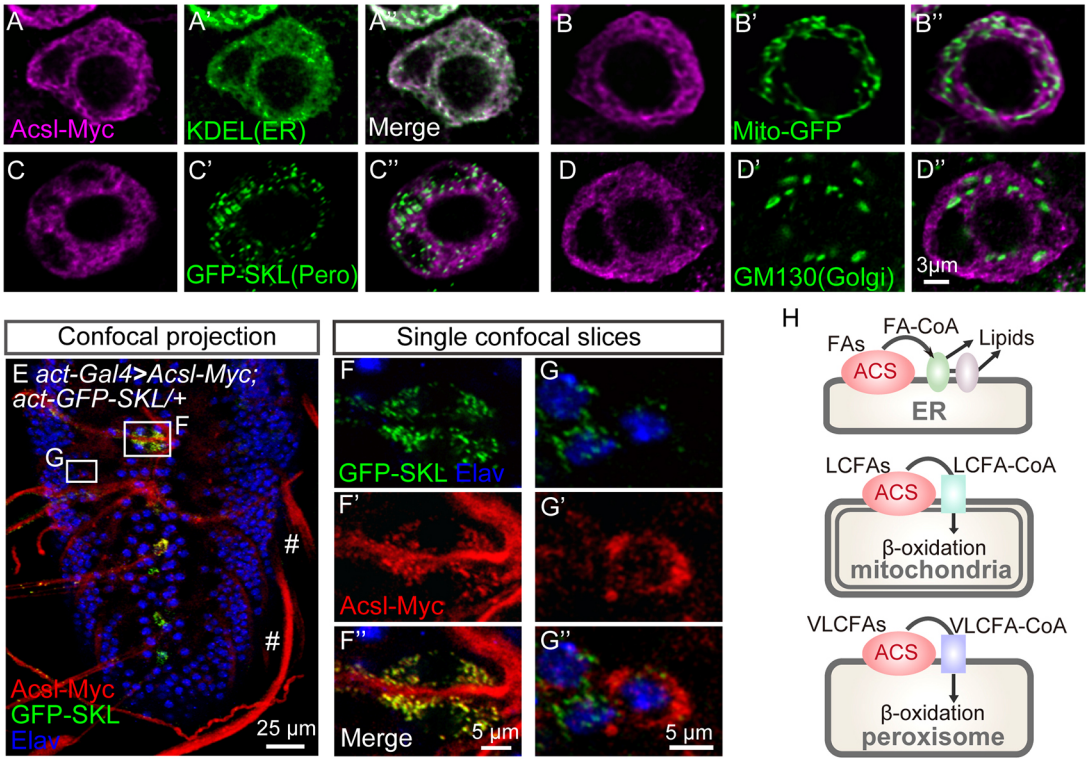

Fig. 2. Acsl localizes at the ER in neurons but at peroxisomes in a subset of non-neuronal cells. (A–D″) Single confocal slices of a motoneuron in the VNC double-labeled for Acsl–Myc (anti-Myc antibody; magenta) and cellular organelle makers (green) including anti-KDEL (A–A″), mito-GFP (B–B″), GFP–SKL (anti-GFP; C–C″) and anti-GM130 (D–D″). Acsl-Myc, mito-GFP and GFP-SKL were expressed in motor neurons by *OK6-Gal4*. (E) Confocal projection of larval ventral nerve cord co-labeled for Acsl–Myc (anti-Myc; red), GFP–SKL (green) and Elav (blue). The genotype is *act-GFP-SKL*/+; *act-Gal4*/*UAS-Acsl-Myc*. # indicates peripheral nerves. (F,G) Single slices at higher magnification and brightness showing the distribution of Acsl–Myc in non-neuronal cells (F–F″) and neurons (G–G″). (H) Schematic representation of the different functions of ACSs in lipid metabolism depending on the specific organelles where ACSs are localized.

the Acsl–Myc signal fully overlapped with GFP–SKL in non-neuronal cells (Fig. 1G–G″). Given that LCFAs are β-oxidized predominantly in mitochondria, whereas β-oxidation of very-long-chain fatty acids (VLCFAs; with 20 and more carbon chains) occurs exclusively in peroxisomes (Wanders and Waterham, 2006), it is possible that Acsl might channel VLCFAs into peroxisomal degradation in a few non-neuronal cells.

Acsl regulates brain fatty acid composition

Mammalian ACSL4 has a substrate preference for arachidonic acid (C20:4) and eicosapentaenoic acid (C20:5) (Golej et al., 2011; Kang et al., 1997). C20 and C22 polyunsaturated fatty acids are absent in *Drosophila* (Shen et al., 2010). To further understand how Acsl affects the fatty acid metabolism, we analyzed fatty acids in third-instar larval brains of $Acsl^{KO}/Acsl^{05847}$ mutants. The brain lobes of these mutants were smaller than those of wild type, and ubiquitous or neuronal overexpression of human ACSL4 fully restored the brain size (data not shown). We examined fatty acid composition from brain lipid extracts by gas chromatography and mass spectrometry (GC-MS) (Christie, 1989). Most fatty acids are trans-esterified from neutral lipids and membrane glycerol-phospholipids (GPLs) but not sphingolipids, whereas a small fraction is esterified from free fatty acids due to their low levels in *Drosophila* (Christie, 1989; Hammad et al., 2011). We analyzed the relative proportion of abundant LCFAs including palmitic acid (C16:0), palmitoleic acid (C16:1), stearic acid (C18:0), oleic acid (C18:1) and linoleic acid (C18:2). Lauric acid (C12:0) and myristic acid (C14:0) were not examined in this study due to their low endogenous levels. The relative abundance of C16:1 and C18:2 was reduced, whereas that of C16:0 was increased in *Acsl*-mutant brains (Fig. 3A,B). Overexpression of human ACSL4 by *tub-Gal4* in $Acsl^{KO}/Acsl^{05847}$ mutants restored C16:1 but not C18:2 levels (Fig. 3C), suggesting that both Acsl and ACSL4 positively regulate C16:1 abundance in larval brains.

Fatty-acid-CoAs are incorporated into lipids in the ER by various acyltransferases (Coleman et al., 2000). We next investigated the levels of C16:1-containing GPLs by high performance liquid chromatography and mass spectrometry (HPLC-MS). The relative level of phosphatidylethanolamine (PtdEth) and phosphatidylcholine (PtdChl) species with C32:1 or C32:2 chains, which primarily contain fatty acyl C16:1, were markedly decreased in *Acsl* mutant brains (Fig. 3D), suggesting that Acsl positively regulates C16:1 level in brain GPLs. These alterations were rescued by ubiquitous expression of Acsl by *tub-Gal4* but not neuronal *elav-Gal4* (Fig. 3D), suggesting that full restoration of C16:1 level in brain GPLs requires ubiquitous Acsl, consistent with the fact that endogenous Acsl is expressed in diverse systems (Zhang et al., 2009). It is probable that Acsl acts in non-neuronal tissues to facilitate the incorporation of exogenous C16:1 into brain lipids.

Reduced C16:1 in *Acsl* mutants contributes to synaptic overgrowth

We speculated that if the reduction in C16:1 fatty acyls contributed to NMJ overgrowth in *Acsl* mutants, then supplementation of C16:1 should suppress the NMJ overgrowth. Because fatty-acid-CoAs are

Journal of Cell Science (2016) 129, 4034-4045 doi:10.1242/jcs.195032

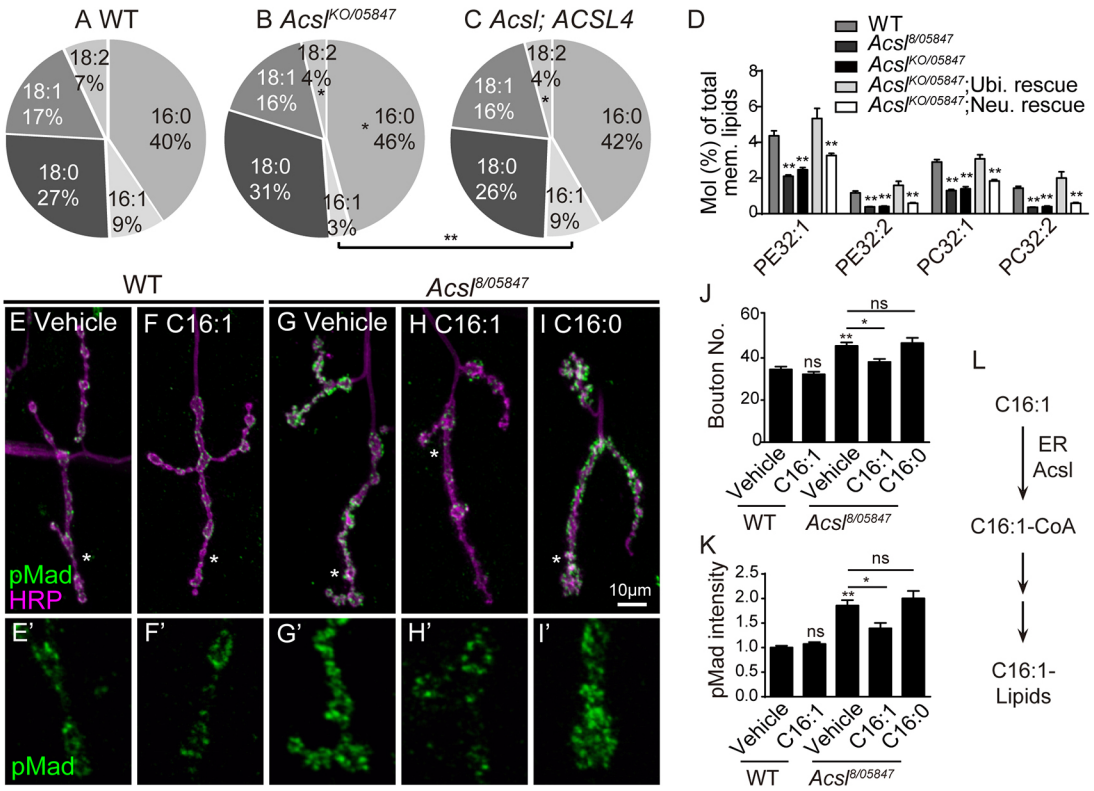

Fig. 3. Acsl regulates fatty acid composition and affects NMJ growth. (A–C) Profiles of abundant fatty acids from third-instar larval brains (including brain lobes and the VNC) from wild-type (A), $Acsl^{KO}/Acsl^{05847}$ (B) and $Acsl^{KO}/Acsl^{05847}$; *tub-Gal4*/*UAS-ACSL4* (C) larvae. *P<0.05; **P<0.01 (ANOVA non-parametric Kruskal–Wallis sum-of-ranks test). (D) Molar fractions of C16:1-containing PtdEth (PE) and PtdChl (PC) species in larval brains from different genotypes. Results are mean±s.e.m. (n=5). WT, wild type. (E–I′) Representative images of NMJ4 labeled with anti-pMad (green) and anti-HRP (magenta) antibodies from wild-type larvae treated with vehicle (0.5% DMSO; E,E') and 1.5% C16:1 fatty acid (F,F′), and $Acsl^{8}/Acsl^{05847}$ treated with vehicle (0.5% DMSO; G,G′), 1.5% C16:1 fatty acid (H,H′),and 1.5% C16:0 fatty acid (I,I′). (J,K) Quantification of bouton number (J) and synaptic anti-pMad intensity normalized to anti-HRP intensity (K) for indicated treatments. Results are mean±s.e.m. (n≥12 larvae). *P<0.05; **P<0.01; ns, not significant (one-way ANOVA with Tukey post hoc tests). (L) Schematic representation of Acsl channeling C16:1 incorporation into lipids in the ER.

not stable in culture media, we next examined the effect of free fatty acids on *Acsl* NMJs. Free fatty acids are substrates of Acsl, thus supplementation of C16:1 might rescue the NMJ defects in weak hypomorphic mutants with residual Acsl activity (Fig. 3L). Feeding larvae with 1.5% C16:1 or C16:0 did not affect NMJ growth in either wild-type or strong hypomorphic $Acsl^{KO}/Acsl^{05847}$ mutants (Fig. 3F,J; data not shown), in which the Acsl protein is undetectable in larval brains (Liu et al., 2014). In contrast, feeding larvae of weak hypomorphic $Acsl^{8}/Acsl^{05847}$ mutants with C16:1 but not C16:0 completely suppressed the NMJ overgrowth (Fig. 3G–J), suggesting that a reduction in C16:1 level might contribute to synaptic overgrowth in *Acsl* mutants.

We previously found that synaptic overgrowth in *Acsl* mutants is due in part to elevated BMP signaling, as evidenced by an increased level of phosphorylated mothers against decapentaplegic (pMad), an effector of BMP signaling at the NMJ (Liu et al., 2014). Here, we found that supplementation of C16:1 but not C16:0 abolished the increase in pMad level in $Acsl^{8}/Acsl^{05847}$ mutants (Fig. 3G′–I′,K), supporting the idea that the reduction in C16:1 level contributes to the increased BMP signaling in *Acsl* mutants.

To confirm that the correct level of C16:1 is required for normal NMJ growth, we examined larvae with mutations that affect C16:1 production. The *Drosophila* stearoyl-CoA desaturase Desat1 catalyzes the desaturation of LCFA-CoAs to produce monounsaturated fatty-acid-CoAs. $desat1^{11}$ mutants (a null mutation) exhibit decreased levels of C16:1 and C18:1 and a correspondingly higher level of C16:0 and C18:0 in membrane GPLs (Kohler et al., 2009). We found that hypomorphic $desat1^{11}/desat1^{EY07679}$ and $desat1^{119}/desat1^{EY07679}$ mutants survived to the third-instar larval stage and showed significant NMJ overgrowth. Expression of Desat1 from a transgenic genomic clone restored NMJ growth in the mutants to control levels (Fig. 4A–F; Fig. S1), indicating that Desat1 inhibits motor neuron bouton formation.

Given that both Desat1 and Acsl positively regulate C16:1 level (Fig. 4G), we speculated that the two enzymes inhibit NMJ growth through a common genetic pathway. RNA interference of *desat1* driven by *tub*-Gal4 resulted in mild NMJ overgrowth. Importantly, NMJ overgrowth upon *desat1* knockdown was significantly enhanced by a heterozygous mutation of $Acsl^{05847}$/+ (Fig. 4H–K,P,Q). Moreover, Desat1 overexpression driven by *act-Gal4* had no effect on bouton number compared with the *act-Gal4* control, but significantly suppressed NMJ overgrowth and abolished the increase in pMad level in $Acsl^{KO}/Acsl^{05847}$ mutants (Fig. 4L–T; Fig. S1). These results demonstrate that Desat1 and Acsl act synergistically to regulate NMJ development, probably by maintaining the balance of fatty acids, especially C16:1.

Raft-related lipid levels are elevated in *Acsl* brains

In addition to affect fatty acid composition, Acsl might modulate the composition of lipid classes by selective activation of different fatty acids in ER. To investigate how Acsl-mediated fatty-acid-CoA

Journal of Cell Science (2016) 129, 4034-4045 doi:10.1242/jcs.195032

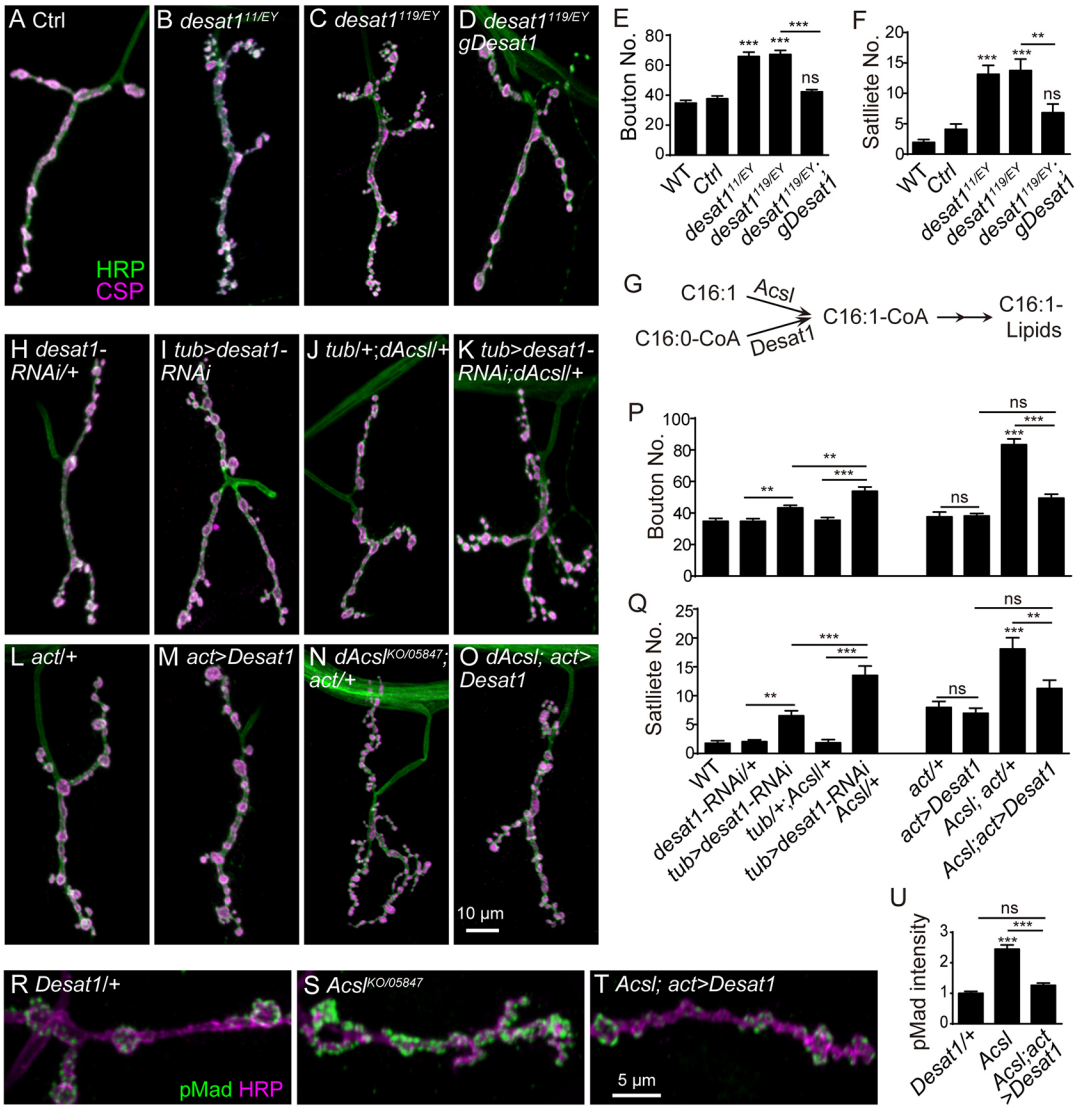

Fig. 4. *Acsl* interacts with *desat1* in regulating NMJ growth. (A–D) Confocal images of NMJ4 labeled with anti-HRP (green) and anti-CSP (magenta) in control (*desat1*^{10}, the precise excision line from *desat1*^{EY07679}; A), *desat1*^{11}/*desat1*^{EY07679} (B) and *desat1*^{119}/*desat1*^{EY07679} (C) larvae and *desat1*^{119}/*desat1*^{EY07679} larvae expressing a transgenic *Desat1* genomic clone (*gDesat1*; *desat1*^{119}/*desat1*^{EY07679}) (D). (E,F) Quantifications of the total bouton number (E) and satellite bouton number (F) of different genotypes. Results are mean±s.e.m. (n≥12 larvae). **P<0.01, ***P<0.001; ns, not significant (one-way ANOVA with Tukey post hoc tests). (G) Schematic representation of Acsl and Desat1 in regulating C16:1-fatty acyl level. (H–O) Images of NMJ4 in segments A2 or A3 co-labeled with anti-HRP (green) and anti-CSP (magenta) in *UAS-desat1-RNAi*/+ (H), *tub-Gal4*/*UAS-desat1-RNAi* (I), *Acsl*^{05847}/+; *tub-Gal4*/+ (J) and *Acsl*^{05847}/+; *tub-Gal4*/*UAS-desat1-RNAi* (K), *act-Gal4*/+ (L), *act-Gal4*/*UAS-desat1* (M), *Acsl*^{KO}/*Acsl*^{05847}; *act-Gal4*/+ (N) and *Acsl*^{KO}/*Acsl*^{05847}; *act-Gal4*/*UAS-desat1* (O) larvae. (P,Q) Quantifications of the total bouton number (P) and satellite bouton number (Q) of various genotypes. Results are mean±s.e.m. (n≥12 larvae). **P<0.01, ***P<0.001; ns, not significant (one-way ANOVA with Tukey post hoc tests). (R–T) Images of NMJ4 co-labeled with anti-pMad (green) and anti-HRP (magenta) from *UAS-desat1*/+ (R), *Acsl*^{KO}/*Acsl*^{05847} (S) and *Acsl*^{KO}/*Acsl*^{05847}; *act-Gal4*/*UAS-desat1* (T) larvae. (U) Quantifications of synaptic anti-pMad intensity normalized to that of anti-HRP from different genotypes. Results are mean±s.e.m. (n≥12 larvae). **P<0.01, ***P<0.001; ns, not significant (one-way ANOVA with Tukey post hoc tests).

synthesis affects lipid composition in the nervous system, we analyzed the membrane lipidome from third-instar larval brains of *Acsl* mutants by HPLC-MS. We analyzed 10 major membrane lipid classes, including four classes of GPLs, PtdEth, PtdChl, phosphatidylinositol (PtdIns) and phosphatidylserine (PtdSer); four classes of sphingolipids, ceramide (Cer), ceramide phosphatidylethanolamine (CerPE), glucosylceramide (GlcCer) and mannosyl glucosylceramide (MacCer); and two sterols, cholesterol and ergosterol. Results for each lipid class were normalized to the sum of tested lipids and are represented as the molar percentage (mol%) of total membrane lipid (Fig. 5A; Table S1). Heat maps depicting ratios of lipid levels between the indicated genotypes were generated to assess changes in lipid abundance (Fig. 5B,D,E).

The level of PtdEth, the most abundant membrane lipid, was decreased in both *Acsl*^{8}/*Acsl*^{05847} and *Acsl*^{KO}/*Acsl*^{05847} larval brains. In contrast, the level of two sphingolipids, CerPE and MacCer, was significantly increased in *Acsl* mutants (Fig. 5A). The MacCer level showed the greatest change in *Acsl*^{KO}/*Acsl*^{05847} mutants relative to the wild type (2.8-fold increase; Fig. 5B; Table S1). The level of ergosterol, the major sterol in *Drosophila*, was also increased in *Acsl* mutants (Fig. 5A). Sphingolipids and sterols assemble into detergent-resistant membrane microdomains known as ‘lipid rafts’ (Lingwood and Simons, 2010; Rietveld et al., 1999); hence, the

Journal of Cell Science (2016) 129, 4034-4045 doi:10.1242/jcs.195032

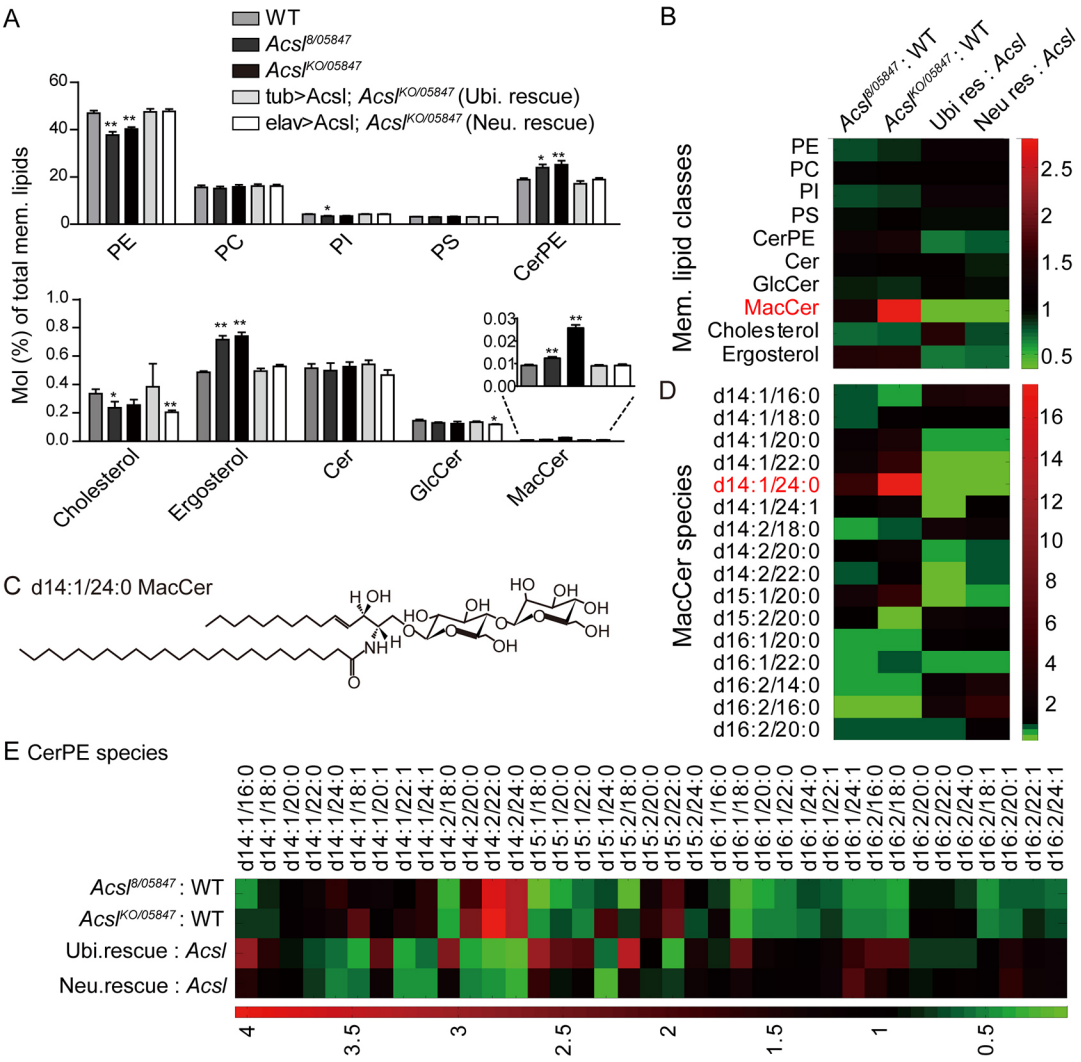

Fig. 5. Levels of raft-related lipids are increased in *Acsl* mutant brains. (A) Lipidomic analysis of membrane lipids in larval brains from wild-type (WT), *Acsl*^{8}/*Acsl*^{05847}, *Acsl*^{KO}/*Acsl*^{05847}, *Acsl*^{KO}/*Acsl*^{05847}; *tub-Gal4*/*UAS-Acsl* (Ubi. rescue) and *Acsl*^{KO}/*Acsl*^{05847}; *elav-Gal4*/*UAS-Acsl* (Neu. rescue). Bar graphs show molar fractions of different lipid classes. PtdEth (PE), PtdChl (PC), PtdIns (PI), PtdSer (PS) and phosphoethanolamine ceramide (CerPE) were relatively abundant (>1%), whereas cholesterol, ergosterol, ceramide (Cer), glucosylceramide (GlcCer) and mannosyl glucosylceramide (MacCer) were present at low levels (<1%). Results are mean±s.e.m. (n=5). *P<0.05, **P<0.01 between indicated genotypes and wild type (ANOVA non-parametric Kruskal–Wallis sum-of-ranks test). (B) Heat maps showing ratios of representative lipid classes between different genotypes. Colors represent ratio values. Lipids in ubiquitous or neural rescue larvae were compared with those in *Acsl*^{KO}/*Acsl*^{05847} mutants. (C) Schematic illustration of d14:1/C24:0 MacCer, which showed the greatest increase among all the individual lipids examined in *Acsl*^{KO}/*Acsl*^{05847} mutants. (D,E) Heat maps showing ratios of individual species of MacCer (D) and individual species of CerPE (E) compared between different genotypes. Levels of MacCer or CerPE species with C14 sphingoid bases and VLCFAs showed the greatest increase in *Acsl* mutants.

altered lipid profiles suggested that membrane lipid raft formation might be increased in *Acsl* mutants. The alteration in membrane lipid composition in *Acsl*^{KO}/*Acsl*^{05847} brains was rescued by ubiquitous or neuronal expression of *Acsl* under the control of *tub-Gal4* and *elav-Gal4*, respectively (Fig. 5A), indicating that abnormal lipid composition is specifically caused by loss of Acsl.

Given that fatty acid moieties in sphingolipids cannot be trans-esterified (Christie, 1989), they were not previously analyzed by the aforementioned GC-MS (Fig. 3A–C). We therefore examined the fatty acid profile for MacCer and CerPE by HPLC-MS. Fatty acids in sphingolipids were longer and more saturated than those in GPLs (Fig. 5D,E), consistent with previous reports (Carvalho et al., 2012; Rietveld et al., 1999). The levels of individual MacCer and CerPE species containing a 14-carbon-sphingoid base (abbreviated as d14) and a VLCFA acyl chain were markedly elevated (Fig. 5D,E), with a concomitant increase in whole classes of MacCer and CerPE in *Acsl* mutants. Notably, MacCer containing a d14:1 base and a C24 fatty acid acyl chain (d14:1/C24:0; Fig. 5C) showed the most significant increase in *Acsl*^{KO}/*Acsl*^{05847} mutants (17.68 fold; Fig. 5D; Table S1). Taken together, Acsl positively regulates PtdEth level but negatively regulates the level of sphingolipids CerPE and MacCer, especially the VLCFA-containing sphingolipids, directly or indirectly.

Increased levels of MacCer and sterol promote synaptic overgrowth in *Acsl* mutants

A lipidomic analysis showed that the increase in MacCer level was the greatest in *Acsl* mutants in all lipid classes we examined (Fig. 5A,B). Furthermore, the extent of increase in MacCer parallels the severity of NMJ overgrowth in different allelic combinations of

Journal of Cell Science (2016) 129, 4034-4045 doi:10.1242/jcs.195032

Acsl mutants (Fig. 1B,C; Fig. 5A,B), suggesting that the severe NMJ overgrowth observed in $Acsl^{KO}/Acsl^{05847}$ mutants might be due to an increased level of MacCer. In addition, a previous study has reported that raft-related lipids are required for normal synapse density and size in cultured hippocampal neurons (Hering et al., 2003). We therefore investigated whether the elevation in MacCer caused NMJ overgrowth in *Acsl* mutants.

Consistent with the lipidomic profiling (Fig. 5A,B), MacCer level showed an obvious increase in $Acsl^{KO}/Acsl^{05847}$ motor neuron NMJs (Fig. 6L,L′,P); this increase was abolished by ubiquitous or neuronal but not muscle expression of Acsl by *Mhc-Gal4* (Fig. 6M,M′,P). Neuronal expression of human ACSL4 by *elav-Gal4* also abrogated the upregulation of MacCer in *Acsl*-mutant NMJs (Fig. 6P).

We next determined whether reducing the level of MacCer could suppress the NMJ overgrowth in *Acsl* mutants. MacCer is generated by the mannosyltransferase Egghead (Egh) and converted into the acetylglucosyl MacCer by the N-acetylglucosaminyl transferase Brainiac (Brn) (Fig. 6R; Wandall et al., 2003, 2005). We found that reducing MacCer level by egh^{62d18} mutation or neuronal overexpression of *brn* by *nSyb-Gal4* resulted in fewer and larger boutons at NMJs (Fig. 6D,I,J,Q). Moreover, a heterozygous $egh^{62d18}/+$ mutation significantly suppressed MacCer elevation and NMJ overgrowth in $Acsl^{KO}/Acsl^{05847}$ mutants, whereas a homozygous egh^{62d18} mutation or *brn* overexpression driven by *nSyb-Gal4* fully restricted the MacCer level and NMJ overgrowth in $Acsl^{KO}/Acsl^{05847}$ mutants (Fig. 6C–F,I,J,N–Q). For example, the bouton number and size in egh^{62d18}; $Acsl^{KO}/Acsl^{05847}$ double mutants were similar to those of egh^{62d18} single mutants (Fig. 6I,J), indicating that synaptic overgrowth in *Acsl* mutants depends on the elevated MacCer level.

A lipidomic analysis revealed that the ergosterol level was significantly increased whereas that of cholesterol was decreased in *Acsl* mutants (Fig. 5A); the sum of ergosterol and cholesterol was nonetheless higher (1.16-fold in $Acsl^{8}/Acsl^{05847}$ and 1.21-fold in $Acsl^{KO}/Acsl^{05847}$) than in wild type. Like MacCer, sterol is also a constituent of lipid rafts and plays a crucial role in synapse development (Hering et al., 2003; Mauch et al., 2001; Rietveld et al., 1999); thus, we determined whether sterol depletion could suppress the NMJ overgrowth in *Acsl* mutants. *Drosophila* does not

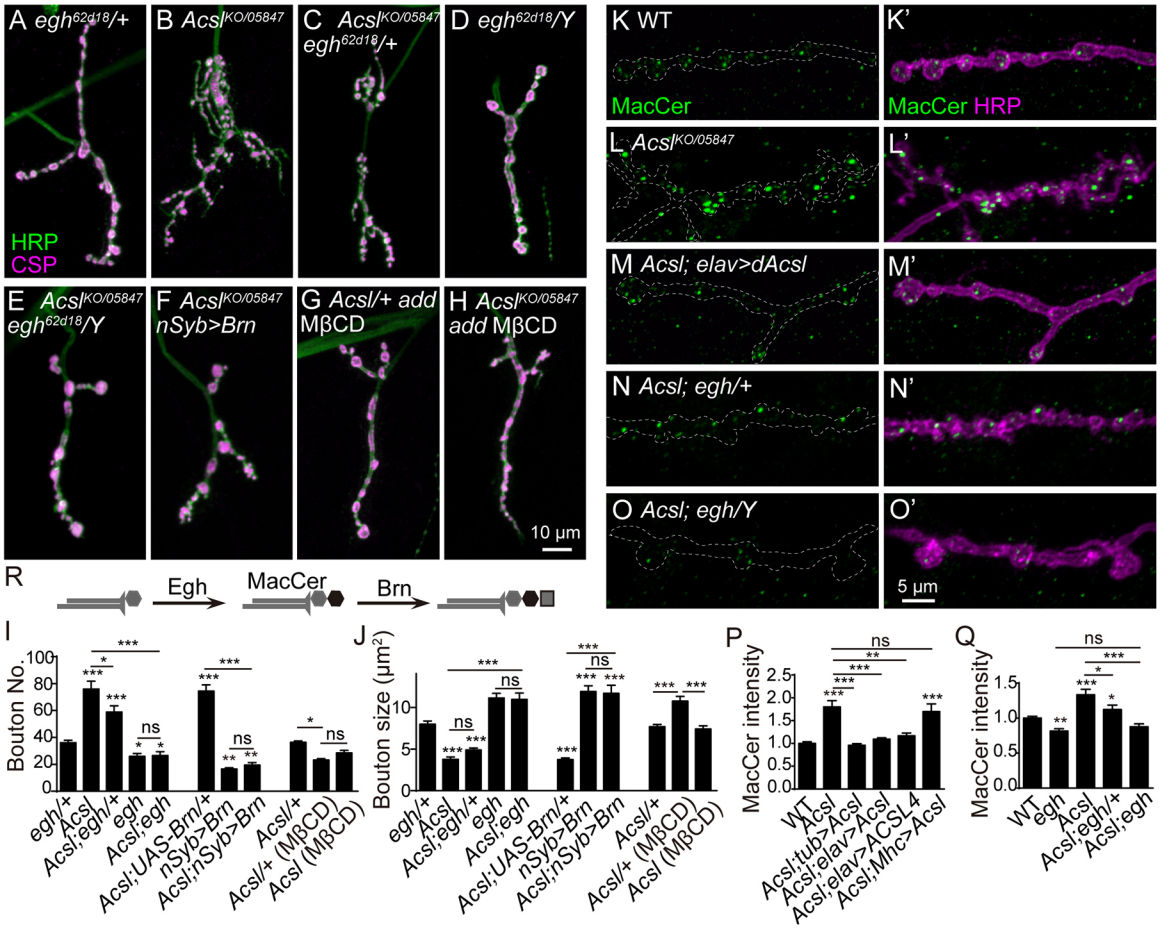

Fig. 6. Reduction in MacCer or sterol level suppresses NMJ overgrowth in *Acsl* mutants. (A–H) Images of representative NMJ4 co-labeled with anti-HRP (green) and anti-CSP (magenta) in $egh^{62d18}/+$ (A), $Acsl^{KO}/Acsl^{05847}$ (B), $egh^{62d18}/+$; $Acsl^{KO}/Acsl^{05847}$ (C), egh^{62d18}/Y (D), egh^{62d18}/Y; $Acsl^{KO}/Acsl^{05847}$ (E), $Acsl^{KO}/Acsl^{05847}$; *UAS-brn/nSyb-Gal4* (F), $Acsl^{KO}/+$ treated with 20 mM MβCD (G) and $Acsl^{KO}/Acsl^{05847}$ treated with 20 mM MβCD (H) larvae. (I, J) Quantification of bouton number (I) and bouton size (J) of NMJs in different genotypes. Results are mean±s.e.m. ($n \geq 12$ larvae). *$P<0.05$, **$P<0.01$, ***$P<0.001$; ns, not significant (one-way ANOVA with Tukey post hoc tests). (K–O′) Representative images of NMJ4 terminals co-labeled with anti-MacCer (green) and anti-HRP (magenta) in wild-type (WT, K,K′), $Acsl^{KO}/Acsl^{05847}$ (L,L′), *elav-Gal4*/+; $Acsl^{KO}/Acsl^{05847}$; *UAS-Acsl*/+ (M, M'), $egh^{62d18}/+$; $Acsl^{KO}/Acsl^{05847}$ (N,N') and egh^{62d18}/Y; $Acsl^{KO}/Acsl^{05847}$ (O,O′) larvae. (P,Q) Quantification of anti-MacCer intensities normalized to that of HRP within presynaptic boutons from different genotypes. Results are mean±s.e.m. ($n \geq 12$ larvae). *$P<0.05$, **$P<0.01$, ***$P<0.001$; ns, not significant (one-way ANOVA with Tukey post hoc tests). (R) Schematic illustration of the metabolism of MacCer. Hexagons of different shades and squares represent sugar residues attached to the scaffold of ceramide.

Journal of Cell Science (2016) 129, 4034-4045 doi:10.1242/jcs.195032

synthesize sterols, which are obtained from yeast-containing food (Carvalho et al., 2010); we therefore used methyl-β-cyclodextrin (MβCD), a cyclic oligosaccharide that efficiently decreases sterol level in various cell lines (Hebbar et al., 2008; Sharma et al., 2004). Feeding control larvae ($Acsl^{KO}$/+) with 20 mM MβCD resulted in fewer and larger boutons at NMJs, whereas NMJ overgrowth was fully suppressed in $Acsl^{KO}/Acsl^{05847}$ mutants by MβCD treatment (Fig. 6G–J). Thus, an excess of sterol might contribute to the NMJ overgrowth in *Acsl* mutants. These results together suggest that increased levels of raft-related MacCer and ergosterol underlie the NMJ overgrowth in *Acsl* mutants.

Acsl regulates C16:1 and MacCer to inhibit synaptic growth in parallel genetic pathways

The above results demonstrate that Acsl regulates the levels of C16:1 and MacCer to inhibit synaptic growth. We next investigated whether there is a mechanistic link between reduced C16:1 and increased MacCer in *Acsl* mutant brains. C16:1 acyl chains were very limited and below the detection limit in sphingolipid species (Fig. 5D,E), suggesting that the reduction in C16:1 in *Acsl* mutants might not directly affect sphingolipid level. In addition, the synaptic staining of MacCer was largely normal in $desat1^{119}/desat1^{EY07679}$ mutants with impaired activity in producing C16:1-CoA (Fig. 7L–N). Finally, unlike in egh^{62d18}; $Acsl^{KO}/Acsl^{05847}$ double mutants, egh^{62d18}; $desat1^{119}/desat1^{EY07679}$ double mutants showed more numerous and smaller synaptic boutons than *egh* mutants (Fig. 7G–J; Fig. S1), suggesting that the NMJ overgrowth in *desat1* mutants likely did not depend on the MacCer level. Although we could not exclude the possibility that the decrease in C16:1 might indirectly influence MacCer level, these results suggest that the increase in MacCer level in *Acsl* mutants might not result from a reduction in C16:1.

The above results suggest that the reduction of C16:1 in *Acsl* mutants is associated with an increase in NMJ growth-promoting BMP signaling (Fig. 3G–K). To determine whether MacCer level also affects BMP signaling, we first analyzed the pMad level. Contrary to expectation based on reduced bouton number, pMad level was unchanged in *Brn*-overexpressing larvae whereas it was significantly increased in egh^{62d18} mutants (Fig. 7K). Furthermore, egh^{62d18} mutation or *brn* overexpression did not efficiently suppress the pMad increase in $Acsl^{KO}/Acsl^{05847}$ mutants

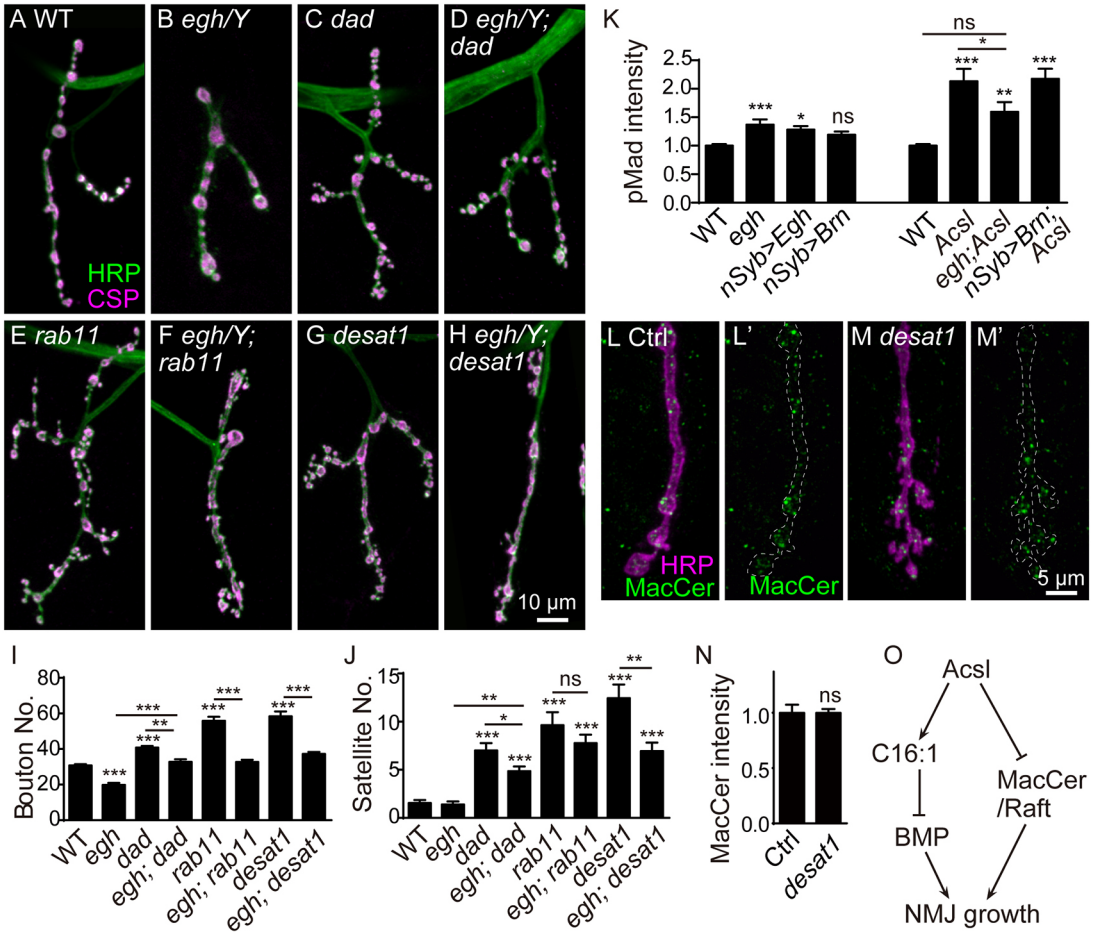

Fig. 7. MacCer and C16:1 fatty acid regulate NMJ growth in parallel genetic pathways. (A–H) Images of NMJ4 co-labeled with anti-HRP (green) and anti-CSP (magenta) in wild-type (WT, A), egh^{62d18}/Y (B), dad^{j1E4} (C), egh^{62d18}/Y; dad^{j1E4} (D), $rab11^{93Bi}$ (E), egh^{62d18}/Y; $rab11^{93Bi}$ (F), $desat1^{119}/desat1^{EY07679}$ (G) and egh^{62d18}/Y; $desat1^{119}/desat1^{EY07679}$ (H) larvae. (I,J) Quantification of the total bouton number (I) and satellite bouton number (J) of NMJ4. Results are mean±s.e.m. ($n \geq 12$ larvae). *P<0.05, **P<0.01, ***P<0.001; ns, not significant (one-way ANOVA with Tukey post hoc tests). (K) Quantifications of pMad intensities within synaptic boutons normalized to HRP intensities of different genotypes. Results are mean±s.e.m. ($n \geq 12$ larvae). *P<0.05, **P<0.01, ***P<0.001; ns, not significant [Student's *t*-test between a test genotype and wild-type (left), and one-way ANOVA with Tukey post hoc tests (right)]. (L–M′) Images of NMJ4 co-stained with anti-MacCer (green) and anti-HRP (magenta) from control (L–L′) and $desat1^{119}/desat1^{EY07679}$ mutants (M–M′). (N) Quantifications of MacCer intensities within boutons normalized to HRP staining intensities of different genotypes. Results are mean±s.e.m. ($n \geq 12$ larvae). ns, not significant (Student's *t*-test). (O) Model of the genetic pathway involving Acsl, C16:1 and MacCer that regulates NMJ growth.

Journal of Cell Science (2016) 129, 4034-4045 doi:10.1242/jcs.195032

(Fig. 7K). These results together show that restriction of NMJ overgrowth in *Acsl* mutants by reducing MacCer does not act through BMP signaling.

BMP signaling is negatively regulated by Daughters against decapentaplegic (Dad) and Rab11, a small GTPase involved in endosomal recycling. Loss-of-function mutations in *dad* or *rab11* result in elevated BMP signaling and synaptic overgrowth (Liu et al., 2014; O'Connor-Giles et al., 2008). To clarify the relationship between MacCer and BMP signaling, we examined the effects of egh^{62d18} mutation on NMJ growth in dad^{j1E4} and $rab11^{93Bi}$ mutants. If the NMJ overgrowth in dad^{j1E4} and $rab11^{93Bi}$ mutants depends on normal levels of MacCer, then egh^{62d18} mutation would be expected to suppress NMJ overgrowth in these mutants to the level of egh^{62d18} single mutants. However, total and satellite bouton numbers in both egh^{62d18}; dad^{j1E4} and egh^{62d18}; $rab11^{93Bi}$ double mutants were significantly more than those observed in *egh* single mutants (Fig. 7A–F,I,J). These data suggest that MacCer acts, at least in part, in a pathway parallel to BMP signaling to promote NMJ growth. Taken together, our findings reveal that Acsl orchestrates a genetic pathway that inhibits NMJ growth by enhancing C16:1 abundance but restricting MacCer level (Fig. 7O).

DISCUSSION

A reduced level of C16:1 fatty acid contributes to NMJ overgrowth in *Acsl* mutants

Like ACSL4, Acsl primarily associates with the ER and facilitates fatty acid incorporation into lipids (Golej et al., 2011; Kuch et al., 2014; Meloni et al., 2009; Zhang et al., 2009); impairment of Acsl activity reduces the abundance of its substrate LCFAs in lipids. Although we did not directly determine the substrate preference of Acsl, our fatty acid analysis suggests that both Acsl and ACSL4 positively regulate C16:1 abundance in *Drosophila* brain (Fig. 3). The two proteins also have conserved functions in other processes, such as lipid storage (Zhang et al., 2009), axonal transport and synaptic development (Liu et al., 2014, 2011).

The similar NMJ overgrowth in *desat1* and *Acsl* mutants suggests that the normal fatty acid composition is essential for proper development of synapses. The rescue effect of C16:1, together with the genetic interaction between *Acsl* and *desat1* (Figs 3 and 4), indicates that reduced C16:1 contributes to NMJ overgrowth in *Acsl* mutants. We previously reported that the synaptic overgrowth in *Acsl* mutants is due in part to an elevation of BMP signaling resulting from defects in endocytic recycling and BMP receptor inactivation (Liu et al., 2014). Endosomes are membrane compartments that are regulated by various membrane lipids (van Meer et al., 2008), particularly the conversion between different PtdIns species, such as PI(3)P, $PI(4,5)P_2$, $PI(3,4,5)P_3$ and so on (Di Paolo and De Camilli, 2006; Lauwers et al., 2016; Kelley et al., 2015). Here, our findings suggest that increased BMP signaling in *Acsl* mutants is associated with an imbalance in fatty acid composition, specifically, a decrease in C16:1. It is thus possible that proper fatty acid composition is necessary for the normal conversion and localization of endosomal lipids (e.g. PtdIns species), affecting endosomal recycling and BMP receptor inactivation. Future studies will examine the regulation of specific fatty acids such as C16:1 in endosomal recycling and BMP signaling.

Acsl regulates lipid class composition

Acsl primarily associates with the ER in multiple cell types including motor neurons and participates in lipid synthesis (Fig. 2A; O'Sullivan et al., 2012; Zhang et al., 2009). In *Drosophila*, most of acyl chains in GPLs are C16 and C18 LCFAs without VLCFAs (Hammad et al., 2011; Rietveld et al., 1999). In contrast, sphingolipids contain higher levels of VLCFAs than LCFAs as acyl chains (Lingwood and Simons, 2010; Rietveld et al., 1999). Thus, most LCFA-CoAs are channeled into GPLs whereas VLCFA-CoAs are mainly incorporated into sphingolipids in *Drosophila*. We found, here, that Acsl positively regulates the production of C16:1-containing GPLs, as well as the level of PtdEth, the most abundant GPL in the brain (Figs 3 and 5). Presumably, fatty acids that are less preferred by Acsl could be channeled into lipids by other ACSs, and might show increased abundance because of a compensatory mechanism in *Acsl* mutants, which could contribute to the elevation in VLCFA-containing sphingolipids (Fig. 5D–E).

In addition to ER localization, ACSL4 and Acsl also localize to peroxisomes in a few non-neuronal cells (Lewin et al., 2002; Fig. 1Q–Q″), suggesting a role for these proteins in the activation of VLCFAs for peroxisomal degradation. Indeed, in animal models and patients with impaired peroxisomal function, accumulation of VLCFAs or increased levels of lipid species with longer fatty acid chains is observed (Chen et al., 2010; Faust et al., 2014; Wanders and Waterham, 2006). Thus, a defect in peroxisomal VLCFA degradation might underlie the elevation in sphingolipid species with VLCFA chains in *Acsl* mutant brains (Fig. 5).

Alternatively, Acsl might affect lipid composition through a pathway that is independent of fatty acid incorporation. For example, as degradation of sphingolipids occurs primarily within lysosomes (Xu et al., 2010), a defect in lysosomal degradation might lead to an accumulation of sphingolipids and sterols in *Acsl* mutants. In addition, fatty acids and acyl-CoAs are ligands of many transcription factors (Ellis et al., 2010; Schroeder et al., 2008), and ACSL3 activates the transcription of lipogenic genes in rat hepatocytes (Bu et al., 2009). Thus, Acsl might transcriptionally regulate genes encoding enzymes involved in the metabolism of lipids such as MacCer, CerPE and PtdEth. However, the detailed mechanism of how Acsl affects lipid class composition, especially the downregulation of raft-related MacCer and CerPE by Acsl in the nervous system, remains to be elucidated.

Raft-related lipids promote synapse growth

Our data showed that elevation of the raft-related lipids MacCer and sterol facilitate NMJ overgrowth in *Acsl* mutants (Fig. 6). Moreover, MacCer promotes bouton formation in a pathway parallel to BMP signaling, at least in part (Fig. 7). It is unclear how these raft-related lipids regulate synaptic growth. It is likely that MacCer and sterol might interact with raft-associated growth signaling pathways. Larval NMJ development is mediated by multiple growth factors and downstream signaling cascades (Collins and DiAntonio, 2007; Deshpande and Rodal, 2016), some of which are activated or modulated by membrane lipid rafts (Allen et al., 2007; Hryniewicz-Jankowska et al., 2014). For instance, Wingless (Wg) (Wnt1 in mammals) is a raft-associated protein (Zhai et al., 2004) that activates signaling pathways essential for NMJ growth and synaptic differentiation (Packard et al., 2002). It is therefore possible that the level or activity of some raft-associated growth factors is increased in *Acsl* mutants, thereby promoting NMJ overgrowth. Further investigation is needed to dissect the regulatory mechanisms of raft-related lipids, particularly MacCer, in promoting synaptic growth and bouton formation. It also would be of interest to address how Acsl-regulated lipids regulate neurotransmission in conjunction with synapse development.

Journal of Cell Science (2016) 129, 4034-4045 doi:10.1242/jcs.195032

MATERIALS AND METHODS

Drosophila stains and genetics

Flies were cultured on standard cornmeal medium at 25°C. w^{1118} was used as the wild type. $Acsl^{8}$, $Acsl^{05847}$, $Acsl^{KO}$, *UAS-Acsl.715.Myc*, *UAS-ACSL4.L.Myc*, *UAS-ACSL4.P375L.Myc* and *UAS-ACSL4.R570S.Myc* were as described previously (Zhang et al., 2009; Liu et al., 2014). $desat1^{10}$ (the precise excision line from $desat1^{EY07679}$), $desat1^{11}$, $desat1^{119}$, $desat1^{EY07679}$ and genomic *desat1* (Kohler et al., 2009) were provided by Ernst Hafen (Institute of Molecular Systems Biology, Swiss Federal Institute of Technology, Zürich, Switzerland). egh^{62d18} and *UAS-Brn* (Chen et al., 2007) were provided by Stephen M. Cohen (Institute of Molecular and Cell Biology, Singapore). *GFP-SKL* under the control of *actin*-promotor (Chen et al., 2010) was from Xun Huang (Institute of Genetics and Developmental Biology, Chinese Academy of Sciences, Beijing, China). The following fly lines were obtained from the Bloomington Stock Center: *UAS-desat1*, *UAS-desat1-RNAi*, *UAS-GFP-SKL*, *UAS-mito-GFP*, *elav-Gal4*, *nSyb-Gal4*, *tub-Gal4*, *act-Gal4*, *OK6-Gal4*, *Mhc-Gal4*, dad^{j1E4} and $rab11^{93Bi}$.

Immunohistochemical staining

Immunostaining of larval preparations was performed as previously described (Liu et al., 2011, 2014). Specimens were dissected in Ca^{2+}-free HL3 saline. For most antibody stainings, samples were fixed in 4% paraformaldehyde for 30–60 min, and washed in 0.2% Triton X-100 in phosphate-buffered saline (PBS). For MacCer staining, specimens were permeabilized with 0.1% Triton X-100 in cold PBS, incubated with undiluted mouse monoclonal anti-MacCer hybridoma supernatants (Hans Wandall, Department of Cellular and Molecular Medicine, University of Copenhagen, Denmark) (Wandall et al., 2005) for 18 h at 4°C and detected with Alexa-Fluor-568-conjugated goat anti-mouse IgM (1:1000; Invitrogen). Other antibodies used were: rabbit anti-pMad PS1 (1:500; Peter ten Dijke, Leiden University, Leiden, Netherlands) (Persson et al., 1998), mouse anti-CSP (1:300; 6D6, DSHB), rat anti-KDEL (1:300; ab50601; Abcam), rabbit anti-GM130 (1:500; ab30637; Abcam), mouse anti-Myc (1:300; CW0259B; CWBIO), rabbit anti-Myc (1:200; M047-3; MBL), mouse anti-Elav (1:100; 9F8A9, DSHB), rat anti-GFP (1:300; D153-3; MBL) and FITC-conjugated anti-horseradish-peroxidase (HRP; 1:200; Jackson ImmunoResearch). Primary antibodies were visualized using specific secondary antibodies conjugated to Alexa Fluor 488, Cy3 (both at 1:1000; Invitrogen) or DyLight 649 (1:500; Jackson ImmunoResearch).

Imaging and data analysis

Images were collected with an Olympus Fluoview FV1000 confocal microscope using a 40×1.42 NA or 60×1.42 NA oil objective and FV10-ASW software, or with a Leica confocal microscope using a 40×1.25 NA oil objective and LAS AF software. All images of muscle 4 type Ib NMJ from abdominal segments A2 or A3 for a specific experiment were captured using identical settings for statistical comparison among different genotypes. Brightness, contrast and color were adjusted using Photoshop CS5 (Adobe). NMJ features were quantified using ImageJ (National Institutes of Health, Bethesda, MD). For quantification of NMJ morphological phenotypes, individual boutons were defined according to the discrete staining signal of anti-CSP antibody. Satellite boutons were defined as extensions of five or fewer small boutons emanating from the main branch of the NMJ terminals (Liu et al., 2014). For quantification of bouton sizes, synaptic areas (μm^2) were measured by assessing HRP-positive boutons, and normalized to bouton numbers. For quantification of MacCer and pMad levels, mean intensities of fluorescence were measured within HRP-positive NMJs, and normalized to that of HRP. These NMJ features were measured by an experimenter that was blind to the genotype. Statistical comparisons were performed using GraphPad Prism 6. Data of NMJ features are expressed as mean±standard error of the mean (s.e.m.). Statistical significance between each genotype and the controls was determined by a two-tailed Student's *t*-test, whereas multiple comparison between genotypes was determined by one-way ANOVA with a Tukey post hoc test. Asterisks above a column indicate comparisons between a specific genotype and control, whereas asterisks above a bracket denote comparisons between two specific genotypes [ns, not significant ($P>0.05$); *$P<0.05$; **$P<0.01$; ***$P<0.001$].

Fatty acid analysis

Fifty third-instar larval brains from a specific genotype were dissected and lysed in cold PBS. Fatty acids were trans-esterified by 2.5% sulfuric acid and methanol. Samples were heated in an 80°C water bath for 2 h and cooled to room temperature, then 2 ml 0.9% sodium chloride and 1 ml hexane was added, extracting fatty acyl methyl esters for analysis (Christie, 1989). Pentadecanoic acid (C15:0; Sigma) was used as an internal standard. GC-MS analysis of fatty acids was performed as previously described (Chen et al., 2010). Gas chromatography was performed using a BPX-70 column (30 m by 0.25 mm, 0.25 µm thickness). Peaks were assigned by using mass spectrometry (Turbomass) to identify fatty acids by both the retention time and fragmentation pattern. Quantification of each fatty acids was performed by an ANOVA non-parametric Kruskal–Wallis sum-of-ranks test for four biological repeats for each genotype (no asterisk denotes $P>0.05$; *$P<0.05$, **$P<0.01$).

Lipidomics of larval brain

Lipids extraction from 10 third-instar larval brains was carried out following the protocols described previously (Lam et al., 2014). Briefly, lipids were extracted with 750 µl of a chloroform and methanol mix (1:2, v/v) and vortexed for 1 min. The samples were placed on a thermomixer and shaken at 1000 rpm for 1 h at 4°C, then 250 µl of chloroform and 350 µl of deionized water were added and vortexed; the lower organic phase was collected after centrifuging at 7600 ***g*** for 2 min. Lipidomic analysis was performed on an Agilent 1260 HPLC system coupled with a triple quadrupole and ion trap mass spectrometer (5500Qtrap, Sciex) (Lam et al., 2014). Individual lipid species were quantified by referencing to spiked internal standards (Avanti Polar Lipids, Alabaster, AL, and Echelon Biosciences, Inc. Salt Lake City, UT). For all HPLC-MS analyses, individual peaks were manually examined and only peaks above the limit of quantification and within the linearity range were used for quantification. Quantification of each lipid species was performed by an ANOVA non-parametric Kruskal–Wallis sum-of-ranks test for five biological repeats for each genotype (no asterisk denotes $P>0.05$, *$P<0.05$, **$P<0.01$).

Drug or fatty acid treatment of larvae

Larvae of different genotypes were raised on vehicle or drug-containing medium from egg hatching, and third-instar larvae were collected for specific analysis. Methyl-fatty acids (C16:1 and C16:0; Sigma-Aldrich) or drugs (Triacsin C and Rosiglitazone; Sigma-Aldrich) were dissolved in DMSO and then added to standard medium at specific concentrations. All the treatments used DMSO vehicle at a concentration of 0.5%. MβCD (Sigma-Aldrich) was resolved in standard medium at a final concentration of 20 mM.

Acknowledgements

We thank H. Wandall, P. ten Dijke, S. M. Cohen, S. Pizette, and E. Hafen, X. Huang for providing antibodies and fly lines. We thank Z. M. Hu for assisting in the GC-MS assay.

Competing interests

The authors declare no competing or financial interests.

Author contributions

Y.H. and Y.Q.Z. designed the research. Y.H., S.H., S.M.L. and Z.H.L. performed the experiments. Y.H., S.H., S.M.L., Z.H.L. G.H.S. and Y.Q.Z. analyzed data. Y.H. and Y.Q.Z. wrote the paper.

Funding

This work was supported by grants from the Ministry of Science and Technology of the People's Republic of China [grant numbers 2014CB942803, 2016YFA0501000]; the Strategic Priority Research Program B of the Chinese Academy of Sciences [grant number XDB02020400]; and the National Science Foundation of China [grant number 31110103907 and 31490590 to Y.Q.Z., 31500846 to Y.H.].

Supplementary information

Supplementary information available online at
http://jcs.biologists.org/lookup/doi/10.1242/jcs.195032.supplemental

References

Allen, J. A., Halverson-Tamboli, R. A. and Rasenick, M. M. (2007). Lipid raft microdomains and neurotransmitter signalling. *Nat. Rev. Neurosci.* **8**, 128-140.

Bazinet, R. P. and Layé, S. (2014). Polyunsaturated fatty acids and their metabolites in brain function and disease. *Nat. Rev. Neurosci.* **15**, 771-785.

Bu, S. Y., Mashek, M. T. and Mashek, D. G. (2009). Suppression of long chain acyl-CoA synthetase 3 decreases hepatic de novo fatty acid synthesis through decreased transcriptional activity. *J. Biol. Chem.* **284**, 30474-30483.

Carvalho, M., Schwudke, D., Sampaio, J. L., Palm, W., Riezman, I., Dey, G., Gupta, G. D., Mayor, S., Riezman, H., Shevchenko, A. et al. (2010). Survival strategies of a sterol auxotroph. *Development* **137**, 3675-3685.

Carvalho, M., Sampaio, J. L., Palm, W., Brankatschk, M., Eaton, S. and Shevchenko, A. (2012). Effects of diet and development on the Drosophila lipidome. *Mol. Syst. Biol.* **8**, 600.

Chen, Y.-W., Pedersen, J. W., Wandall, H. H., Levery, S. B., Pizette, S., Clausen, H. and Cohen, S. M. (2007). Glycosphingolipids with extended sugar chain have specialized functions in development and behavior of Drosophila. *Dev. Biol.* **306**, 736-749.

Chen, H., Liu, Z. and Huang, X. (2010). Drosophila models of peroxisomal biogenesis disorder: peroxins are required for spermatogenesis and very-long-chain fatty acid metabolism. *Hum. Mol. Genet.* **19**, 494-505.

Christie, W. W. (1989). *Gas Chromatography and Lipids: a Practical Guide*. Ayr, Scotland: The Oily Press.

Coleman, R. A., Lewin, T. M. and Muoio, D. M. P. (2000). Physiological and nutritional regulation of enzymes of triacylglycerol synthesis. *Annu. Rev. Nutr.* **20**, 77-103.

Collins, C. A. and DiAntonio, A. (2007). Synaptic development: insights from Drosophila. *Curr. Opin. Neurobiol.* **17**, 35-42.

Davletov, B. and Montecucco, C. (2010). Lipid function at synapses. *Curr. Opin. Neurobiol.* **20**, 543-549.

Deshpande, M. and Rodal, A. A. (2016). The crossroads of synaptic growth signaling, membrane traffic and neurological disease: insights from Drosophila. *Traffic* **17**, 87-101.

Di Paolo, G. and De Camilli, P. (2006). Phosphoinositides in cell regulation and membrane dynamics. *Nature* **443**, 651-657.

Ellis, J. M., Frahm, J. L., Li, L. O. and Coleman, R. A. (2010). Acyl-coenzyme A synthetases in metabolic control. *Curr. Opin. Lipidol.* **21**, 212-217.

Faust, J. E., Manisundaram, A., Ivanova, P. T., Milne, S. B., Summerville, J. B., Brown, H. A., Wangler, M., Stern, M. and McNew, J. A. (2014). Peroxisomes are required for lipid metabolism and muscle function in Drosophila melanogaster. *PLoS ONE* **9**, e100213.

Golej, D. L., Askari, B., Kramer, F., Barnhart, S., Vivekanandan-Giri, A., Pennathur, S. and Bornfeldt, K. E. (2011). Long-chain acyl-CoA synthetase 4 modulates prostaglandin E2 release from human arterial smooth muscle cells. *J. Lipid. Res.* **52**, 782-793.

Hammad, L. A., Cooper, B. S., Fisher, N. P., Montooth, K. L. and Karty, J. A. (2011). Profiling and quantification of Drosophila melanogaster lipids using liquid chromatography/mass spectrometry. *Rapid Commun. Mass Spectrom.* **25**, 2959-2968.

Hebbar, S., Lee, E., Manna, M., Steinert, S., Kumar, G. S., Wenk, M., Wohland, T. and Kraut, R. (2008). A fluorescent sphingolipid binding domain peptide probe interacts with sphingolipids and cholesterol-dependent raft domains. *J. Lipid Res.* **49**, 1077-1089.

Hering, H., Lin, C. C. and Sheng, M. (2003). Lipid rafts in the maintenance of synapses, dendritic spines, and surface AMPA receptor stability. *J. Neurosci.* **23**, 3262-3271.

Hryniewicz-Jankowska, A., Augoff, K., Biernatowska, A., Podkalicka, J. and Sikorski, A. F. (2014). Membrane rafts as a novel target in cancer therapy. *Biochim. Biophys. Acta* **1845**, 155-165.

Kang, M.-J., Fujino, T., Sasano, H., Minekura, H., Yabuki, N., Nagura, H., Iijima, H. and Yamamoto, T. T. (1997). A novel arachidonate-preferring acyl-CoA synthetase is present in steroidogenic cells of the rat adrenal, ovary, and testis. *Proc. Natl. Acad. Sci. USA* **94**, 2880-2884.

Kelley, C. F., Messelaar, E. M., Eskin, T. L., Wang, S., Song, K., Vishnia, K., Becalska, A. N., Shupliakov, O., Hagan, M. F., Danino, D. et al. (2015). Membrane charge directs the outcome of F-BAR domain lipid binding and autoregulation. *Cell Rep.* **13**, 2597-2609.

Kim, J. H., Lewin, T. M. and Coleman, R. A. (2001). Expression and characterization of recombinant rat Acyl-CoA synthetases 1, 4, and 5. Selective inhibition by triacsin C and thiazolidinediones. *J. Biol. Chem.* **276**, 24667-24673.

Kniazeva, M., Shen, H. L., Euler, T., Wang, C. and Han, M. (2012). Regulation of maternal phospholipid composition and IP3-dependent embryonic membrane dynamics by a specific fatty acid metabolic event in C. elegans. *Gene Dev.* **26**, 554-566.

Köhler, K., Brunner, E., Guan, X. L., Boucke, K., Greber, U. F., Mohanty, S., Barth, J. M. I., Wenk, M. R. and Hafen, E. (2009). A combined proteomic and genetic analysis identifies a role for the lipid desaturase Desat1 in starvation-induced autophagy in Drosophila. *Autophagy* **5**, 980-990.

Küch, E.-M., Vellaramkalayil, R., Zhang, I., Lehnen, D., Brügger, B., Sreemmel, W., Ehehalt, R., Poppelreuther, M. and Füllekrug, J. (2014). Differentially localized acyl-CoA synthetase 4 isoenzymes mediate the metabolic channeling of fatty acids towards phosphatidylinositol. *Biochim. Biophys. Acta Mol. Cell Biol.* **1841**, 227-239.

Lam, S. M., Wang, Y., Duan, X., Wenk, M. R., Kalaria, R. N., Chen, C. P., Lai, M. K. P. and Shui, G. (2014). The brain lipidomes of subcortical ischemic vascular dementia and mixed dementia. *Neurobiol. Aging* **35**, 2369-2381.

Lauwers, E., Goodchild, R. and Verstreken, P. (2016). Membrane lipids in presynaptic function and disease. *Neuron* **90**, 11-25.

Lewin, T. M., Van Horn, C. G., Krisans, S. K. and Coleman, R. A. (2002). Rat liver acyl-CoA synthetase 4 is a peripheral-membrane protein located in two distinct subcellular organelles, peroxisomes, and mitochondrial-associated membrane. *Arch. Biochem. Biophys.* **404**, 263-270.

Lingwood, D. and Simons, K. (2010). Lipid rafts as a membrane-organizing principle. *Science* **327**, 46-50.

Liu, Z., Huang, Y., Zhang, Y., Chen, D. and Zhang, Y. Q. (2011). Drosophila acyl-CoA synthetase long-chain family member 4 regulates axonal transport of synaptic vesicles and is required for synaptic development and transmission. *J. Neurosci.* **31**, 2052-2063.

Liu, Z., Huang, Y., Hu, W., Huang, S., Wang, Q., Han, J. and Zhang, Y. Q. (2014). dAcsl, the Drosophila ortholog of acyl-CoA synthetase long-chain family member 3 and 4, inhibits synapse growth by attenuating bone morphogenetic protein signaling via endocytic recycling. *J. Neurosci.* **34**, 2785-2796.

Longo, I., Frints, S. G., Fryns, J. P., Meloni, I., Pescucci, C., Ariani, F., Borghgraef, M., Raynaud, M., Marynen, P., Schwartz, C. et al. (2003). A third MRX family (MRX68) is the result of mutation in the long chain fatty acid-CoA ligase 4 (FACL4) gene: proposal of a rapid enzymatic assay for screening mentally retarded patients. *J. Med. Genet.* **40**, 11-17.

Mashek, D. G., Li, L. O. and Coleman, R. A. (2007). Long-chain acyl-CoA synthetases and fatty acid channeling. *Future Lipidol.* **2**, 465-476.

Meloni, I., Muscettola, M., Raynaud, M., Longo, I., Bruttini, M., Moizard, M.-P., Gomot, M., Chelly, J., des Portes, V., Fryns, J.-P. et al. (2002). FACL4, encoding fatty acid-CoA ligase 4, is mutated in nonspecific X-linked mental retardation. *Nat. Genet.* **30**, 436-440.

Meloni, I., Parri, V., De Filippis, R., Ariani, F., Artuso, R., Bruttini, M., Katzaki, E., Longo, I., Mari, F., Bellan, C. et al. (2009). The XLMR gene ACSL4 plays a role in dendritic spine architecture. *Neuroscience* **159**, 657-669.

Mauch, D. H., Nägler, K., Schumacher, S., Göritz, C., Müller, E.-C., Otto, A. and Pfrieger, F. W. (2001). CNS synaptogenesis promoted by glia-derived cholesterol. *Science* **294**, 1354-1357.

Najmabadi, H., Hu, H., Garshasbi, M., Zemojtel, T., Abedini, S. S., Chen, W., Hosseini, M., Behjati, F., Haas, S., Jamali, P. et al. (2011). Deep sequencing reveals 50 novel genes for recessive cognitive disorders. *Nature* **478**, 57-63.

O'Connor-Giles, K. M., Ho, L. L. and Ganetzky, B. (2008). Nervous wreck interacts with thickveins and the endocytic machinery to attenuate retrograde BMP signaling during synaptic growth. *Neuron* **58**, 507-518.

O'Sullivan, N. C., Jahn, T. R., Reid, E. and O'Kane, C. J. (2012). Reticulon-like-1, the Drosophila orthologue of the Hereditary Spastic Paraplegia gene reticulon 2, is required for organization of endoplasmic reticulum and of distal motor axons. *Hum. Mol. Genet.* **21**, 3356-3365.

Packard, M., Koo, E. S., Gorczyca, M., Sharpe, J., Cumberledge, S. and Budnik, V. (2002). The drosophila wnt, wingless, provides an essential signal for pre- and postsynaptic differentiation. *Cell* **111**, 319-330.

Persson, U., Izumi, H., Souchelnytskyi, S., Itoh, S., Grimsby, S., Engstrom, U., Heldin, C. H., Funa, K. and ten Dijke, P. (1998). The L45 loop in type I receptors for TGF-beta family members is a critical determinant in specifying Smad isoform activation. *FEBS Lett.* **434**, 83-87.

Rietveld, A., Neutz, S., Simons, K. and Eaton, S. (1999). Association of sterol- and glycosylphosphatidylinositol-linked proteins with Drosophila raft lipid microdomains. *J. Biol. Chem.* **274**, 12049-12054.

Schroeder, F., Petrescu, A. D., Huang, H., Atshaves, B. P., McIntosh, A. L., Martin, G. G., Hostetler, H. A., Vespa, A., Landrock, D., Landrock, K. K. et al. (2008). Role of fatty acid binding proteins and long chain fatty acids in modulating nuclear receptors and gene transcription. *Lipids* **43**, 1-17.

Sharma, P., Varma, R., Sarasij, R. C., Ira, Gousset, K., Krishnamoorthy, G., Rao, M. and Mayor, S. (2004). Nanoscale organization of multiple GPI-anchored proteins in living cell membranes. *Cell* **116**, 577-589.

Shen, L. R., Lai, C. Q., Feng, X., Parnell, L. D., Wan, J. B., Wang, J. D., Li, D., Ordovas, J. M. and Kang, J. X. (2010). Drosophila lacks C20 and C22 PUFAs. *J. Lipid. Res.* **51**, 2985-2992.

Sivachenko, A., Gordon, H. B., Kimball, S. S., Gavin, E. J., Bonkowsky, J. L. and Letsou, A. (2016). Neurodegeneration in a Drosophila model of Adrenoleukodystrophy: the roles of the bubblegum and double bubble acyl-CoA synthetases. *Dis. Model. Mech.* **9**, 377-387.

Van Horn, C. G., Caviglia, J. M., Li, L. O., Wang, S., Granger, D. A. and Coleman, R. A. (2005). Characterization of recombinant long-chain rat acyl-CoA synthetase isoforms 3 and 6: identification of a novel variant of isoform 6. *Biochemistry* **44**, 1635-1642.

van Meer, G., Voelker, D. R. and Feigenson, G. W. (2008). Membrane lipids: where they are and how they behave. *Nat. Rev. Mol. Cell. Biol.* **9**, 112-124.

Journal of Cell Science

Wandall, H. H., Pedersen, J. W., Park, C., Levery, S. B., Pizette, S., Cohen, S. M., Schwientek, T. and Clausen, H. (2003). Drosophila egghead encodes a beta 1,4-mannosyltransferase predicted to form the immediate precursor glycosphingolipid substrate for brainiac. *J. Biol. Chem.* **278**, 1411-1414.

Wandall, H. H., Pizette, S., Pedersen, J. W., Eichert, H., Levery, S. B., Mandel, U., Cohen, S. M. and Clausen, H. (2005). Egghead and brainiac are essential for glycosphingolipid biosynthesis in vivo. *J. Biol. Chem.* **280**, 4858-4863.

Wanders, R. J. A. and Waterham, H. R. (2006). Biochemistry of mammalian peroxisomes revisited. *Annu. Rev. Biochem.* **75**, 295-332.

Watkins, P. A., Maiguel, D., Jia, Z. and Pevsner, J. (2007). Evidence for 26 distinct acyl-coenzyme A synthetase genes in the human genome. *J. Lipid Res.* **48**, 2736-2750.

Xu, Y.-H., Barnes, S., Sun, Y. and Grabowski, G. A. (2010). Multi-system disorders of glycosphingolipid and ganglioside metabolism. *J. Lipid Res.* **51**, 1643-1675.

Zhai, L., Chaturvedi, D. and Cumberledge, S. (2004). Drosophila Wnt-1 undergoes a hydrophobic modification and is targeted to lipid rafts, a process that requires porcupine. *J. Biol. Chem.* **279**, 33220-33227.

Zhang, Y., Chen, D. and Wang, Z. (2009). Analyses of mental dysfunction-related ACSl4 in Drosophila reveal its requirement for Dpp/BMP production and visual wiring in the brain. *Hum. Mol. Genet.* **18**, 3894-3905.

Zhang, H. J., Abraham, N., Khan, L. A., Hall, D. H., Fleming, J. T. and Gobel, V. (2011). Apicobasal domain identities of expanding tubular membranes depend on glycosphingolipid biosynthesis. *Nat. Cell. Biol.* **13**, 1189-1201.

Zhu, H. H., Shen, H. L., Sewell, A. K., Kniazeva, M. and Han, M. (2013). A novel sphingolipid-TORC1 pathway critically promotes postembryonic development in Caenorhabditis elegans. *Elife* **2**, e00429.

Zoghbi, H. Y. and Bear, M. F. (2012). Synaptic dysfunction in neurodevelopmental disorders associated with autism and intellectual disabilities. *Cold Spring Harb. Perspect. Biol.* **4**, a009886.

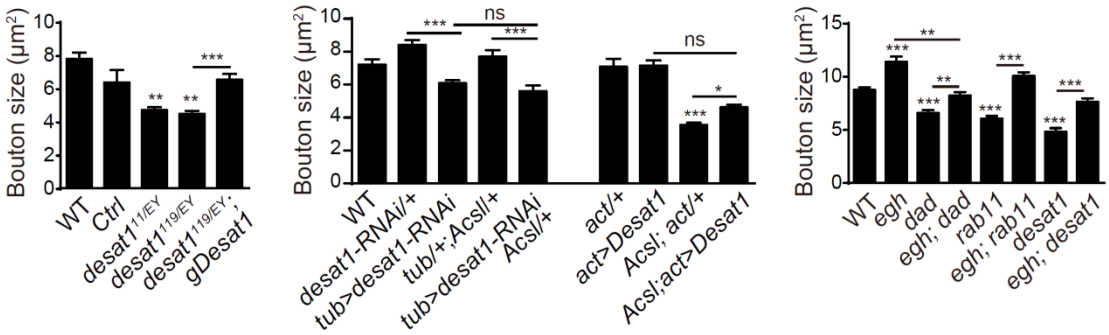

Figure S1. Quantifications of NMJ bouton size.

Quantifications of bouton size of NMJ4 in different genotypes. $n \geq 12$ larvae; ns, no significance; *$P < 0.05$, **$P < 0.01$, ***$P < 0.001$ by one-way ANOVA with Tukey *post hoc* tests; error bars: s.e.m.

Table S1: Lipidomic data of membrane lipids.

Ratio value: ratios of lipid levels between the indicated genotypes to assess changes in lipid abundance; related to Fig. 5B,D,E. **Molecular fraction**: molar percentage (mol%) for each lipid class or species normalized to the sum of lipids measured; 5 biological repeats for each genotype; related to Fig. 3D and Fig. 5. ***P*-value**: comparison of each lipid class or species of indicated genotype to that of wild-type by ANOVA non-parametric Kruskal-Wallis sum-of-ranks; $P < 0.05$ is highlighted by pink; related to Fig. 3D and Fig. 5.

Click here to Download Table S1